Reynolds Number Effects on Fully-Developed Pulsed Jets Impinging on Flat Surfaces

H. Medina*

Coventry University, Coventry, CV1 5FB, United Kingdom

E. Benard†

University of Glasgow, Glasgow, G12 8QQ, United Kingdom

J.M. Early‡

The Queen's University of Belfast, Belfast, BT9 5AH, United Kingdom

To be included

Nomenclature

A_N Pulse amplitude, U_{rms}/U_{avg}
d Nozzle diameter, m
H Nozzle-to-plate spacing, m
Re Reynolds number
r Radial distance from stagnation point, m
St Strouhal number
T_{avg} Average temperature $(T_1 + T_2)/2$, °C
T_r Room temperature, °C
T_1 Experiment start temperature, °C
T_2 Experiment start temperature, °C
U_e Time-averaged centreline exit velocity, m/s
u, v Instantaneous axial and radial velocity components, m/s
u', v' Mean axial and radial turbulent velocity components, m/s
x Axial distance from nozzle exit, m

Subscripts
max Cycle maximum velocity
min Cycle minimum velocity
rms Root mean square
Abbreviations
PIV Particle image velocimetry
TKE Turbulent kinetic energy

I. Introduction

When the development of a free-jet flow (generated when a fluid is discharged from a nozzle into an ambient fluid) is interrupted by the prescence of a surface, an impinging jet is created. Impinging jets are characterised by a rapid deceleration of the discharged fluid as it reaches the surface. This deceleration leads

*Senior Lecturer, Faculty of Engineering and Computing, Coventry University Non-member
†Senior Lecturer, Department of Aerospace Engineering, University of Glasgow
‡Lecturer, The Queen's University of Belfast, AIAA Senior Member

to high rates of momentum, heat and mass transfer, consequently, impinging jets have found a place in many industrial applications (for example, cooling of electronics, inner surfaces of turbine blades, etc).

Due to the numerous practical applications of impinging jets, their study has been mainly oriented towards understanding their mass, momentum and heat transfer characteristics.[1,2] However, an understanding of the underlying fluid mechanics behind these types of jet also offers significant benefits to the study of free shear layers and boundary layers. Furthermore, from a modelling perspective, the study of impinging jets can be incorporated into the development of turbulence models, as most are tested on flows which are parallel to the wall (and as such are not equipped to deal with flows in which the streamlines are orientated close to orthogonal). Even though efforts to improve computational models have been made, they are being held back by the lack of detailed experimental data[3] as a large quantity of the research on impinging jets is still mainly oriented towards understanding the heat transfer characteristics of impinging jets at high Reynolds numbers since they lead to the highest rates of heat transfer.

The study of these jet structures has been further complicated by the numerous configurations which are encountered, which has often led to contradictions in the obsrevations made about their behaviour.[4] Of more interest is the possibility that the use of a pulsating, rather than steady, impinging jet can enhance the heat transfer rates, but again, this has not been conclusively proven and evidence does exist to contradict this, demonstrating the pulsation has a detrimental effect on the heat transfer characteristics.,[5,6].[7] While these discrepancies in the heat transfer characteristics exist, there is in addition a fundamental lack of research on the velocity and turbulent fields of these jet structures. There are only a few works available that study the velocity field of pulsed, but the focus is still firmly on the heat transfer mechanims, with limited velocity data presented. jets.[8,9] It is therefore evident that due to the large number of potential experimental configurations, and the contradictions observed throughout the literature for both steady and pulsating jets, there is a need for both a systematic approach to the study of impinging jets and an in-depth study of the flow field and fluid mechanics. This will not only serve as a basis to understanding how the velocity field might affect heat transfer, but also to provide data for turbulence model validation. The current paper presents the results of an experimental study conducted into the effects of pulsation on the flow field of a turbulent impinging jet, examining the effects of varying the non-dimensional frequency of the pulsation.

II. Experimental Setup and Procedure

A. Experimental Facility

The experiments were undertaken in a custom built water facility at the Queen's University of Belfast. This facility operates on a recirculating principle in which it relies on a gravity-fed mechanism to generate the jet. An overhead tank provides the required head, and the water passes through the pulsator (the valve remains fully opened for the steady jet experiments) and the nozzle inlet, before finally exiting at the test section into the main water tank. The excess water from the main tank is collected into a reservoir tank and is pumped back up to the overhead tank in order to maintain a constant water level in the head tank (necessary to keep a steady supply of water to the test section). A schematic of the experimental apparatus can be seen in figure 1.

The test section is constructed as a rectangular glass tank (inner dimensions 605.6mm long, 302.8mm tall and 300.8mm wide), with a wall thickness of 2mm (capable of holding approximately 55 litres of water). Glass was a convenient material because it allows visual access to the test section.

In order to ensure a fully developed exit profile, a round nozzle (d_inner=30.5mm) of 50 diameters in length was utilised. The first 40 diameters(1,220mm) consist of a straight PVC tube (to prevent rusting and ensure no degradation of the inner wall quality). However, for the last 10 diameters (305mm) of the nozzle a sleeve was used to ensure that the inner section of the nozzle remained circular.

A custom-built pulsator was used to provide the required control over the non-dimensional frequencies tested. The pulsator consists of a rotating valve, a reduction mechanism, and a driving motor. A PB100 (PN25) chromium-plated brass full bore valve (diameter 25mm) was modified so that it could rotate 360 degrees, and therefore interrupt the flow of water (generating two pulses per revolution). The rotating valve was driven using an ABB motor (model M2VA71B-2) rated at 0.55 Kw of power. This 3 phase motor was controlled using a control unit also manufactured by ABB. Once a rotating frequency was selected it was kept constant within ± 0.1 Hz. The maximum frequency at which the motor could be rotated was 47.5 Hz, which translates to a maximum rotating frequency of 2.8 Hz for the valve due to the presence of the reduction mechanism.

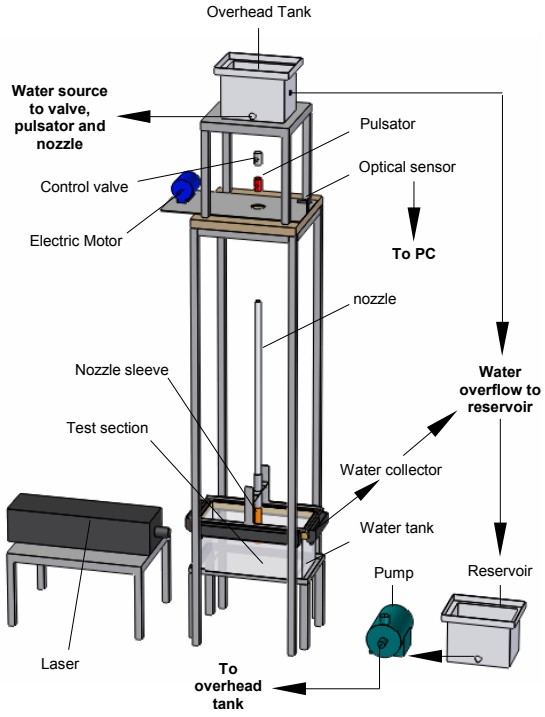

Figure 1. Experimental Facility Overview

B. Data Acquisition

A high-speed PIV system was used in order to acquire time-resolved velocity data. This system is comprised of a laser head, a power supply unit, a chiller (used to cool the laser head), a high-speed camera and a PC. Both the laser head and the power supply unit are manufactured by Lightwave Electronics. The laser head consists of a Nd:YAG laser which produces pulses of a wavelength of 532 nm at a maximum power of 100 mW. The system can be triggered internally and externally; if the system is triggered internally it can be operated at frequencies of up to 100 KHz, externally, it can operate up to 16 KHz. In order to maintain the highest possible camera resolution, a maximum operating frequency chosen was 500 Hz. The camera used to capture the images was a HSS-2 HighSpeedStar Video Camera System (LaVision) was used for image capture. This is single frame CCD digital camera with a storage capacity of 1.28 GB (1022 images at highest resolution). It has a spatial resolution of 1280 pixels by 1024 pixels. The TTL trigger for the pulsed experiments was provided by an optical sensor (Monarch Instrument, Model ROS-5W) pointed at the rotating valve. This sensor is needed so that the images for the pulsed experiments can be taken at the same point in the cycle with an accuracy of 0.005%.

1. Software and Calibration

The image acquistion and post-processing was performed using LaVision Davis 7.0. The calibration plate used was a 80mm x 80 mm laminated card, a white background with 225 black crosses. The distance between cross centroid was 5 millimetres. The choice of interrogation window and post-processing was the same for all experiments. A multi-pass (2) decreasing window size algorithm with a 50% overlap was used. The initial interrogation window size was 128x128 pixels and the final window size was 32x32 pixels. Due to the use of window overlapping, the final spatial resolution is 16 pixels.

2. System Accuracy and Error

With the aid of sub-pixel estimators used in Davis, the PIV system is capable of measuring displacements as small as 0.1 pixel. Therefore, the minimum resolved speed is a function of the camera magnification and the acquisition frequency. Based on the highest acquisition frequency and the largest field of view employed, the system accuracy is $\pm 0.001\ m/s$. There are many factors that can lead to errors in the calculation of the velocity vectors. These include; the choice of particle, out-of-plane motion, high displacement gradients, laser accuracy, peak-locking, etc. By an appropriate selection of particles (size and density) most of the potential sources of errors can be eliminated or neglected. For the work presented, the diameter of the particles was a concern since it is smaller than 2 pixels, therefore, increasing the chance of peak-locking, so anti-peak-locking algorithms were employed. Vectors were calculated using decreasing window sizes and overlapping, therefore significantly reducing (or eliminating) the bias towards small particle displacements in areas with high velocity gradients. Consequently, it was determined that the main source of error in the velocity calculation originated from the calibration of the camera. In regards to the position of the crosses in the calibrating plate, the least accurate mapping function for the experiments carried out in this investigation gave a standard deviation of 0.2 pixel. Assuming a normal distribution of the crosses, and for a 95% confidence level, a given interrogation window will be located within 0.4 pixel of its measured position. Therefore, for a final interrogation window of 32x32 pixels, the estimated error is $\pm 1.25\%$.

C. Data Analysis

Once the velocity data were extracted from the acquired images using Davis 7.0, any further analysis on the data was perform using Matlab. The velocity statistics for the steady jet were obtained using the well known Reynolds decomposition. However, for the pulsed regime, the velocity statistics were obtained using a triple decomposition of the velocity signal.

1. Reynolds Decomposition

The velocity statistics for steady jets were obtained using the Reynolds decomposition of the velocity signal shown in equation (1), where $u_{(x,r)}$ represents the measured velocity, at axial location x, and radial location r, $U_{(x,r)}$ is the local mean of the velocity signal, and $u'_{(x,r)}$ is the fluctuating part of the velocity component. Furthermore, the turbulent part of the velocity signal can be extracted rearranging equation (1), to obtain equation (2). Using this relation, the turbulent statics can be computed at each position (x, r), over the entire data range, N, using the equations shown in table 1, where N, is the number of vector fields. Finally, the time between vector fields corresponds to $1/f$, where f, is the acquisition frequency.

$$u_{(x,r)} = U_{(x,r)} + u'_{(x,r)} \tag{1}$$

$$u'_{(x,r)} = u_{(x,r)} - U_{(x,r)} \tag{2}$$

Statistic Type	**Equations**
Velocity Fluctuations	$u'_{rms(x,r)} = \sqrt{\frac{1}{N}\sum_{i=1}^{N}\left(u_{i(x,r)} - U_{(x,r)}\right)^2}$
Mean TKE	$k_{(x,r)} = \frac{1}{2N}\sum_{i=1}^{N}\left(u_{i(x,r)} - U_{(x,r)}\right)^2 + \left(v_{i(x,r)} - V_{(x,r)}\right)^2$
Reynolds Stresses	$u'v'_{(x,r)} = \frac{1}{N}\sum_{i=1}^{N}\left(u_{i(x,r)} - U_{(x,r)}\right)\left(v_{i(x,r)} - V_{(x,r)}\right)$

Table 1. Turbulent quantities equations used for steady jets

2. *Triple Decomposition*

The velocity signal of the pulsed jets was decomposed using a triple decomposition[10,11] shown in equation (3), where $u_{(x,r)_t}$ is the total velocity or measured velocity, $U_{(x,r)}$ is the time-averaged velocity over all the cycles, $\widetilde{U}_{(x,r)_t}$ is the phase-locked averaged velocity, measured from $U_{(x,r)}$, and finally, $u'_{(x,r)_t}$ is the turbulent or fluctuating component. In addition, x and r, represent the axial and radial locations where the velocity signal is extracted, at time t. In order to reduce computing time, the time-averaged velocity $U_{(x,r)}$, which has a fixed value over time, was combined with the phase-locked average velocity $\widetilde{U}_{(x,r)_t}$ resulting in $\widehat{U}_{(x,r)_t}$, therefore, equation (3), can be rewritten as shown in equation (4), which represents a dual decomposition of the velocity signal. Finally, the turbulent component of the velocity signal can be extracted using equation (5). This process is shown graphically in figure 2. Therefore, $u'_{(x,r)_t}$, represents the turbulent part of the velocity signal at time t of the cycle, but with the cyclic component removed. The relations used in order to calculated the turbulent quantities for pulsed jets are shown in table 2, where N is the total number of velocity fields and t_i represents the time in the cycle that corresponds to a given value of N.

$$u_{(x,r)_t} = U_{(x,r)} + \widetilde{U}_{(x,r)_t} + u'_{(x,r)_t} \tag{3}$$

$$u_{(x,r)_t} = \widehat{U}_{(x,r)_t} + u'_{(x,r)_t} \tag{4}$$

$$u'_{(x,r)_t} = \widehat{U}_{(x,r)_t} - u_{(x,r)_t} \tag{5}$$

Statistic Type	**Equations**
Velocity Fluctuations	$u'_{rms(x,r)} = \sqrt{\frac{1}{N}\sum_{i=1}^{N}(u_{i(x,r)_{t_i}} - \widehat{U}_{(x,r)_{t_i}})^2}$
Triple Correlations	$u'^3_{(x,r)} = \frac{1}{N}\sum_{i=1}^{N}(u_{i(x,r)_{t_i}} - \widehat{U}_{(x,r)_{t_i}})^3$
Mean TKE	$k_{(x,r)} = \frac{1}{2N}\sum_{i=1}^{N}(u_{i(x,r)_{t_i}} - \widehat{U}_{(x,r)_{t_i}})^2 + (v_{i(x,r)_{t_i}} - \widehat{V}_{(x,r)_{t_i}})^2$
Reynolds Stresses	$u'v'_{(x,r)} = \frac{1}{N}\sum_{i=1}^{N}(u_{i(x,r)_{t_i}} - \widehat{U}_{(x,r)_{t_i}})(v_{i(x,r)_{t_i}} - \widehat{V}_{(x,r)_{t_i}})$

Table 2. Turbulent quantities equations used for pulsed jets

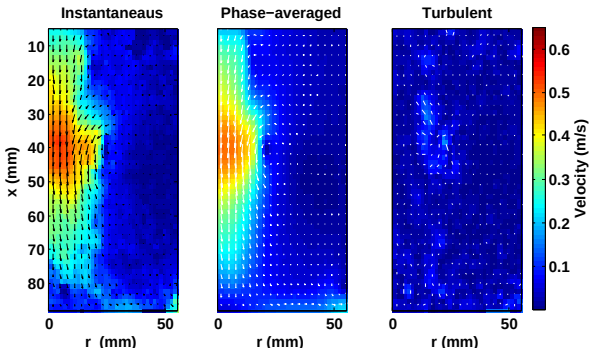

Figure 2. Decomposition of the velocity signal (whole-field)

D. Experimental Error and Uncertainty

Table 3 presents a summary of the estimated error for the various turbulent statistics presented in this work. As already mentioned, the accuracy of the velocity measurements is based on the most limiting experiments carried out, giving an accuracy of 0.001 m/s. Also, the estimated error on the instantaneous and time-averaged velocity measurements was estimated at ±1.25%.

Experimental Quantity	**Associated Error**
instantaneous velocities (u, v)	±1.25%
mean velocities (U, V)	±1.25%
turbulent components (u', v')	±2.00%
velocity fluctuations (u'_{rms}/U_e, v'_{rms}/U_e)	±3.00%
Reynolds stresses ($u'v'/U_e^2$)	±4.50%
TKE (k/U_e^2)	±5.50%

Table 3. Error summary

III. Results and Discussion

The primary aim of the current work is to examine the effect of the non-dimensional frequency, St, on the flow field of turbulent pulsating impinging jets. All the other parameters that affect the flow field of pulsating jets were kept constant ($Re \approx 10200$, $H/d = 3$, and $d = 30.5mm$). The non-dimensional frequency was set at $St = 0$ (steady jet), 0.10 and 0.25 (pulsating jet). A detailed summary of the test conditions is given in table 4

Variables			**Temperatures (°C)**				**Acquisition Information**		**Exit Conditions**			
Re	H/d	St	T_r	T_1	T_2	T_{avg}	Freq. (Hz)	No. Imgs.	U_{min}	U_{max}	U_e	A_N
10000	3	-	19.00	20.50	20.60	20.55	500	3066	-	-	0.330	-
10560	3	0.10	18.00	19.90	20.50	19.75	250	16380	0.121	0.497	0.350	35%
10240	3	0.25	17.90	18.60	19.30	18.95	500	13284	0.223	0.502	0.345	30%

Table 4. Test conditions summary (velocities in m/s)

A. Flow Characterisation

A round nozzle was used in order to provide an axisymmetric jet flow, with the flow demonstrating a good axisymmetry apart from at low Reynolds numbers ($Re < 5,000$), where a slight break in symmetry near the impinging wall for $0.6 < r/d < 1.4$, with a maximum deviation of approximately 18%. This break in symmetry is attributed to laser light reflections present in the near wall region on the left-hand side of the field-of-view which impaired the calculation of the velocity vectors.

The experimental rig was designed to generate impinging jets with a fully developed exit velocity profile. For the steady flow regime, the velocity profiles at exit were fully developed for Reynolds numbers greater than 3,250. However, for the pulsed flow regime, the exit velocity profiles were only fully developed for Reynolds numbers greater than 3,500.

The axial velocity fluctuations at the jet centreline and at 0.5 diameters away from the nozzle exit are shown in figure 3 for a range of different Reynolds numbers. The results of Aydore[12] and Gardon[13] are also shown for comparison. The correlation shown in figure 3 closely fits the values of the velocity fluctuations within the free jet region of impinging jets. For Reynolds numbers ranging from 3500 (transitional) to 15000, the velocity fluctuations in the flow can be related to the Reynolds number by:

$$\frac{u'^2}{U_e} = -3.1x10^{-6}Re + 0.075$$

The correlation to include jets with higher Reynolds numbers would not be a simple straight line because as the Reynolds number increases to $Re > 20000$, the value of u'_{rms}/U_e tends to an asymptotic value of 0.01.[14,15]

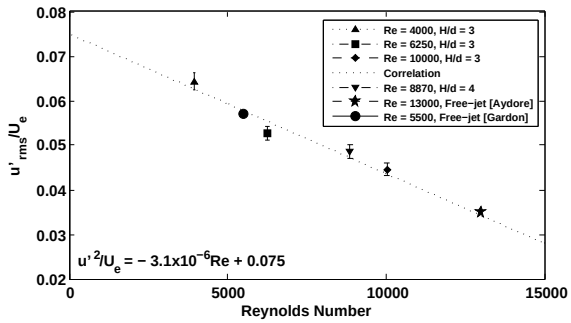

Figure 3. Axial velocity fluctuations in the free jet region ($x/d = 0.5$ and $r/d = 0$)

IV. Effect of the Reynolds Number

A. Introduction

In the preceding sections there was evidence suggesting that the Reynolds number might have a different effect on pulsating jets compared to steady jets, therefore, its effect on pulsating jets will be presented in this section. All the other factors that affect the flow field are kept constant; $H/d = 3$, $St = 0.25$. The diameter of the jet (d) is kept at 30.5mm. The Reynolds numbers for comparison are 4800, 7990 and 10240.

B. Time-Averaged Flow Field

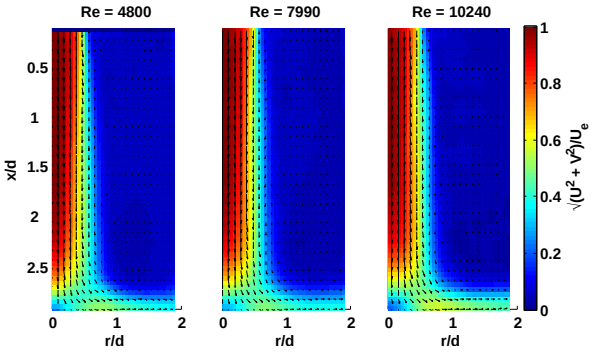

Figure 4. Effect on the Reynolds number on the time-averaged velocity field; closed symbols - steady jet, open symbols pulsed jet ($H/d = 3$, $St = 0.25$)

Fig.4 shows that as the Reynolds number is increased, the core of the jet shortens which was not the case for steady jets. In addition, for steady jets there is an increase in the radial spread rate of the jet as the Reynolds number is increased. This also holds for pulsed jets but the influence of the Reynolds number on the spread rate is moderate. Finally, Fig.4 also shows that as the Reynolds number is increased the wall jet ($r/d > 1$) becomes stronger.

It was found that the centreline axial velocity decay for steady jet does not show a significant reduction up to $x/d = 2$, in contrast, for pulsating jets, it begins to decline at $x/d = 1.5$. In addition, for pulsating jets, the centreline axial velocity component declines more rapidly as the Reynolds number is increased, indicating that the presence of the pulse shortens the core of the jet (Fig.5). However, for steady jets, the Reynolds number does not have a significant effect on the centreline velocity decay (previous chapter).

The effect of the Reynolds number on the development of the axial and radial velocity component is shown in Fig.6. This figure shows that the Reynolds number does not have a strong influence on the development of the axial velocity component. However, the development of the radial velocity component shows that as the Reynolds number is increased (Fig.6c and Fig.6b), the spread rate of the jet increases, although this effect of the Reynolds number is more pronounced for steady jets. It can also be noticed that the presence of a

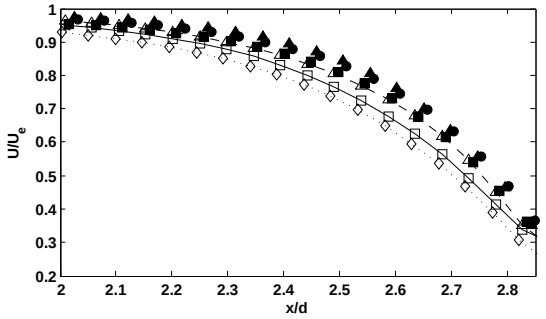

Figure 5. Centreline axial velocity decay; closed symbols - steady jet, open symbols pulsed jet ($H/d = 3$, $St = 0.25$)

pulsation leads to an increase of the jet spread rate in comparison to steady jets (Fig.6b). Interestingly, the most significant influence of the Reynolds number on pulsed jets is found near the impinging wall. Firstly, the presence of a pulsation leads to higher values of the radial velocity component at $r/d > 0.75$ for all jets in comparison to their steady counterpart. Furthermore, the magnitude of the local maximum is not proportional to the Reynolds number, for instance, the jet with $Re = 4200$ exhibits a local maximum larger than the jet with $Re = 7990$, however, it increases for $Re = 10240$, leading to the largest value of V/U_e. This behaviour could be a consequence of significant differences between the vortex rings due to the influence of the Reynolds number. For instance, as the Reynolds number is increased, the vortex rings become stronger, as shown in Fig.7. Also, the Reynolds number affects the way the vortices reach and interact with the wall (Fig.8). For example, for $Re = 4200$ the vortex is weak and does not penetrate the jet wall jet, however, for $Re = 7990$, the vortex penetrates the wall jet. Interestingly, as the Reynolds number is further increased to $Re = 10240$, its vortex is moved away from the wall, probably forced away from the wall by the fluid within the jet core which begins to move radially sooner and faster (Fig.6b), therefore, developing a stronger wall jet which prevents the vortex from penetrating it as deeply as the jet with $Re = 7990$. Finally, the presence of the pulsation fixes the location of the maximum radial velocity component near the wall at approximately $r/d = 0.75$, independently of the Reynolds number, as least for the values of Re tested.

C. Velocity Fluctuations

First of all, Fig.9 shows that, overall, as the Reynolds number is increased, the axial velocity fluctuations decrease. A similar reduction was also encountered for in turbulent pulsating jets as the Strouhal number was increased. In that case, the reduction was due to the strengthening of the vortices which help reduce the turbulent part of the axial velocity component. In this case, not only, the vortices become stronger as the Reynolds number is increased, but also the exit velocity increases, inducing a more pronounced reduction of u'_{rms}/U_e. Similarly, the radial velocity fluctuations (Fig.10) also decrease as Re is increased, although, this decrease is moderate.

The effect of the Reynolds number on the centreline axial velocity fluctuations is shown in Fig.11. It suggests that the effect of the Reynolds number for pulsating jets is not as straight forward as in steady jets, in particular with the jet at the lowest Reynolds number exhibiting velocity fluctuations that fall between the levels of the other two jets, which could be an indication of the transitional nature of such jet. However, this figure shows that there is a steady increase of the centreline velocity fluctuations at $1.25 < x/d < 2.4$ for pulsed jets, up to $r/d \approx 2.4$, where pulsed jets reach higher values of u'_{rms}/U_e than steady jets. In addition, similarly to steady jets, as the Reynolds number is increased, the centreline axial velocity fluctuations near the stagnation point decrease.

Radial profiles of u'_{rms}/U_e at different axial locations are shown in Fig.12. It shows that near the nozzle exit (Fig.12c), the Reynolds number does not have a strong influence on the axial velocity fluctuations. However, the profiles of the pulsed jets are flatter than those of their steady equivalent, also, steady jets exhibit slightly higher peak values. Further downstream, at $x/d = 2.5$ (Fig.12b), the profiles for the pulsed jets are also wider than the steady profiles, showing an increase of u'_{rms}/U_e for $0 < r/d < 0.25$, but also, the Reynolds number has slightly more influence on u'_{rms}/U_e at $0.2 < r/d < 0.6$, leading to a decrease of

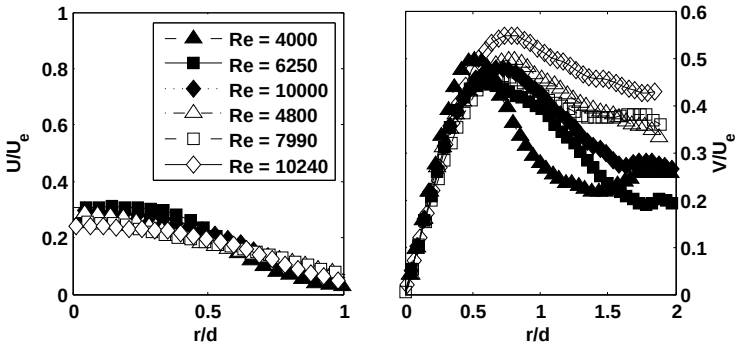

(a) x/d = 2.85

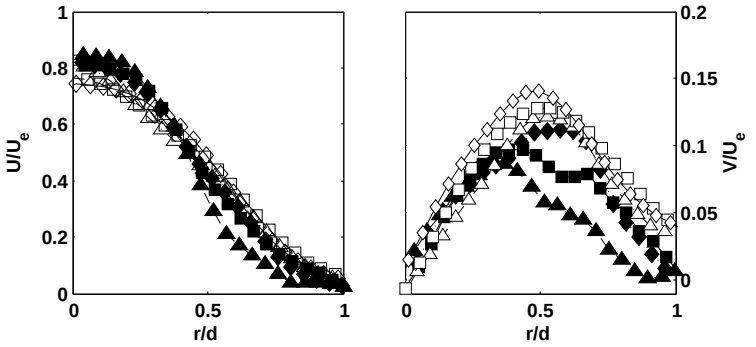

(b) x/d = 2.5

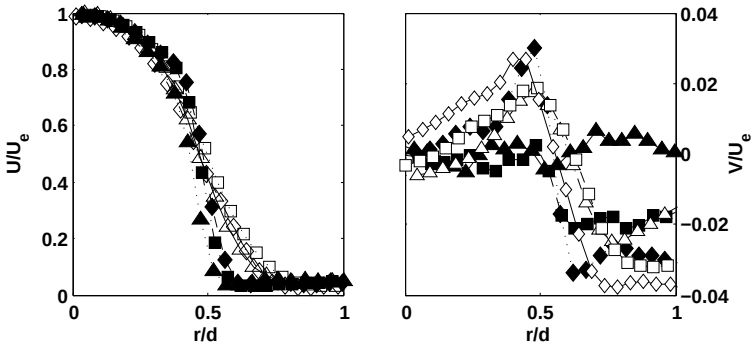

(c) x/d = 0.5

Figure 6. Radial profiles of the mean axial (left) and radial (left) velocity components; closed symbols - steady jet, open symbols pulsed jet ($H/d = 3$, $St = 0.25$)

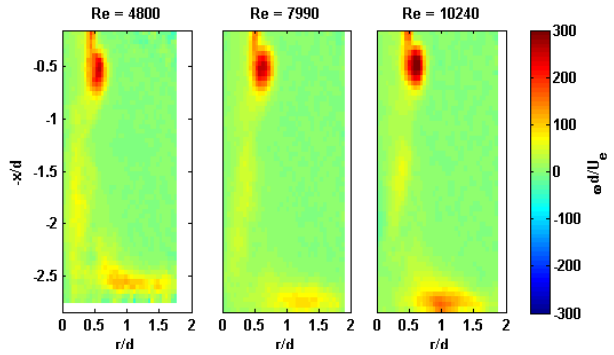

Figure 7. Effect of the Reynolds number on the vorticity field ($H/d = 3$, $St = 0.25$)

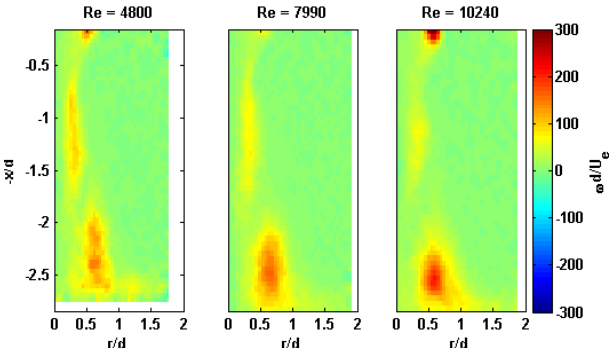

Figure 8. Effect of the Reynolds number on the vorticity field ($H/d = 3$, $St = 0.25$)

the axial velocity fluctuations as it is increased. Furthermore, it is near the impinging wall that the effects of the Reynolds number are most significant as shown in Fig.12a. It shows that as the Reynolds number is increased, there is a significant decrease in the values of u'_{rms}/U_e. It also shows an increase of u'_{rms}/U_e in comparison to steady jets within the stagnation region ($0 < r/d < 0.3$).

Fig.13 shows radial profiles of the radial velocity fluctuations near the wall. It can be observed that for $r/d > 1$ the effect of the Reynolds number on v'_{rms}/U_e is similar to that of steady jets, that is, it reduces the value of v'_{rms}/U_e. However, for steady jets, this is noticeable from $r/d > 0.5$. This indicates that the presence of the pulse, delays the effect of the Reynolds number on v'_{rms}/U_e to $r/d > 0.75$. Also, it can be seen that the presence of the pulsating frequency leads to higher velocity fluctuations of the radial velocity component at $r/d > 0.5$ for the higher Reynolds numbers, and at $r/d > 1$ for the transitional jet.

D. Turbulent Kinetic Energy

Fig.14 shows that the effect of the Reynolds number is rather straight forward, that is, there is a significant decrease in the mean turbulent kinetic energy as the Reynolds number is increased, especially, within the shear layer of the jet. This decrease is mostly due to the decrease of the axial velocity fluctuations as Re is increased, since they have a stronger influence on the mean TKE within the shear layer than the radial velocity fluctuations.

The effect of Re near the impinging wall is explored in Fig.15. It shows, that similarly to steady jets at $0.6 < r/d < 1.5$, the effect of the Reynolds number is to decrease the mean turbulent kinetic energy. Furthermore, for pulsed jets there is a steady increase of the mean TKE for $r/d > 0.9$, whereas, for steady jets, this increase is not evident up to approximately $r/d > 1.5$. Finally, for $Re = 7900$ there is an increase in the values of k/U_e^2 for approximately $0.4 < r/d < 0.9$ when compared to the other jets. This local increase is influenced by the higher values of the radial velocity fluctuations also present at $0.4 < r/d < 0.9$ (Fig. 13 on page 13). The increase in the values of v'_{rms}/U_e for this region could be a result of the vortices being distorted, combined with the fact that the jet vortex rings penetrate the wall jet (see Fig. 8).

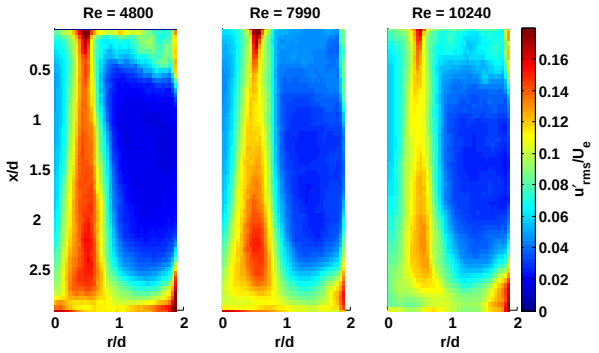

Figure 9. Effect of the Reynolds number on the axial velocity fluctuations ($H/d = 3$, $St = 0.25$)

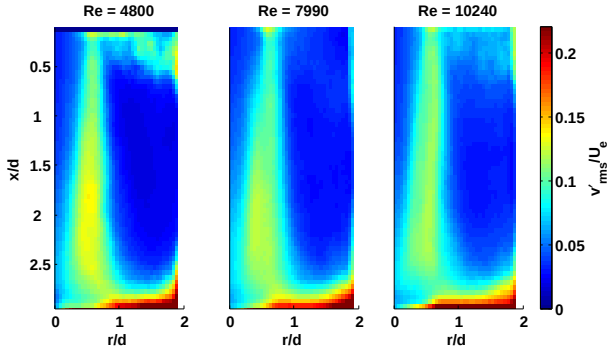

Figure 10. Effect of the Reynolds number on the radial velocity fluctuations ($H/d = 3$, $St = 0.25$)

E. Reynolds Stress

Fig.16 shows the effect of the Reynolds number on pulsating jets, including the type of Reynolds stress induced. First of all, it can be noticed that as the Reynolds number is increased, the Reynolds stress linked to entrainment (en) and expulsion (e) decrease for all jets. Near the impinging wall, the type of Reynolds stresses are similar for all jets, apart from high-speed fluidic interactions away from the wall (O), that are not present for the jet with $Re = 4200$. Therefore, these type of Reynolds stresses are generated at $4200 < Re < 7900$, at least within the radial distance covered in these experiments ($0 < r/d < 2$). Interestingly, as the Reynolds number is increased from $Re = 4800$ to $Re = 7990$, there is an increase in the Reynolds stress (w) near the wall at $1.25 < r/d < 1.80$. This increase is linked to the increase of the radial skewness factor at this location (Fig. **??** on page ??), indicating that the radial turbulent component dominates these low-speed Reynolds stress (W). Finally, it can also be observed that as the Reynolds number is increased from $Re = 7990$ to $Re = 10240$, there is a significant reduction of the Reynolds stress that act away from the wall (O). This decrease is due to a decrease in v'^3/U_e, therefore, this region (O) is dominated by u', which being negative has a direction away from the wall. Consequently, the momentum transport due to this Reynolds stress would have a general directionality away from the impinging wall.

F. Mean Axial Momentum Balance Near the Wall

First of all, Fig.17 shows that the mean momentum transfer, near the impinging wall, for steady jets is larger than that of pulsed jets. Also, it can be noticed, that for the lower Reynolds number, the normal stress term is a sink. However, as the Reynolds number is further increased to $Re = 10240$, they show no contribution to the momentum balance near the wall. This change in the behaviour of the normal stresses could be a result of the reduction exhibited by the entrainment Reynolds stress near the impinging wall as the the Reynolds number is increased (Fig.16). This indicates that for the lower Reynolds numbers, the effect of increased levels of entrainment is translated into a transfer of momentum from the mean to the turbulent field. Fig.17 also shows that as the Reynolds number is increased the contribution to the momentum transport from the

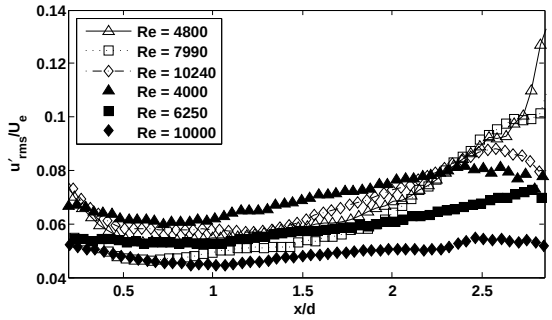

Figure 11. Effect of the Reynolds number on the centreline axial velocity fluctuations; closed symbols - steady jet, open symbols pulsed jet ($H/d = 3$, $St = 0.25$)

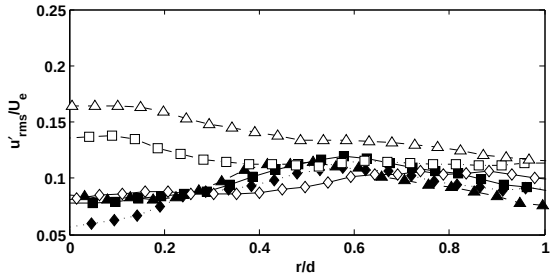

(a) x/d = 2.85

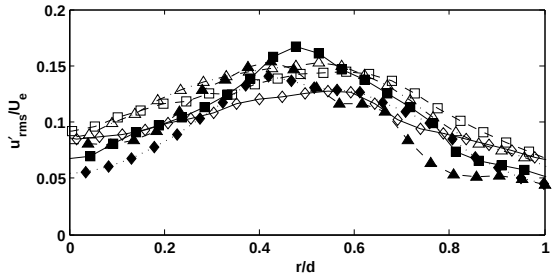

(b) x/d = 2.5

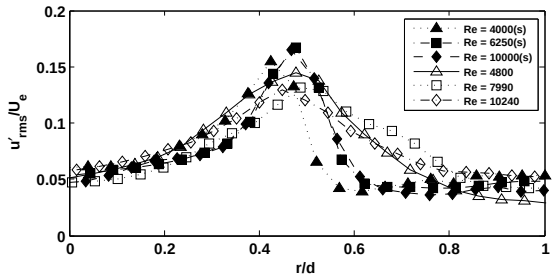

(c) x/d = 0.5

Figure 12. Radial profiles of axial velocity fluctuations; closed symbols - steady jet, open symbols pulsed jet ($H/d = 3$, $St = 0.25$)

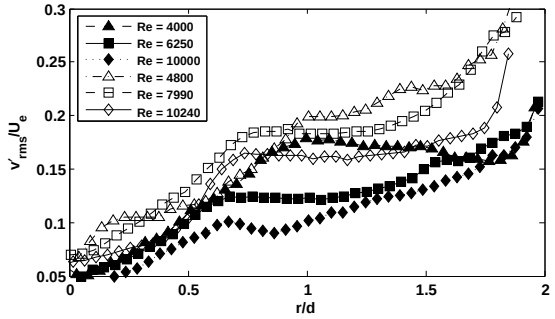

Figure 13. Effect of the Reynolds number on the radial velocity fluctuations near the impinging wall; closed symbols - steady jet, open symbols pulsed jet ($H/d = 3$, $St = 0.25$, $x/d = 2.85$)

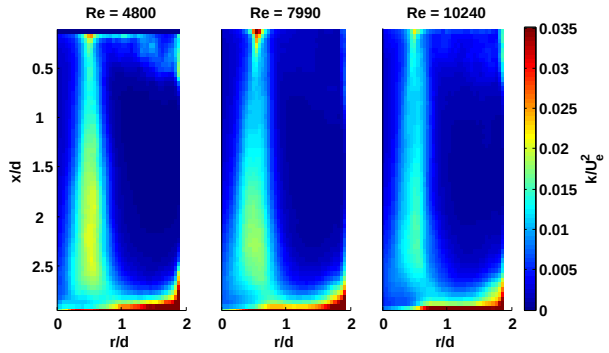

Figure 14. Effect of the Reynolds number on the mean turbulent kinetic energy ($H/d = 3$, $St = 0.25$)

radial diffusion increases, this is direct line with the increase in the values of V/U_e seen in the profile of the mean radial velocity component near the impinging wall (Fig.6a), which leads to increases in the radial diffusion term for $r/d > 0.8$, particularly for $Re = 10240$. This effect is similar to increasing the pulsating frequency for the same reason. This suggests that, an enhancement in the momentum transfer due to the radial diffusion could be achieved by increasing both, the Reynolds number and the Strouhal number.

V. Conclusion

To be included

References

[1]Ma, C. F., Zheng, Q., Lee, S. C., and Gomi, T., "Impingement heat transfer and recovery effect with submerged jets of large Prandtl number liquid - I. Unconfined circular jets," *International journal of heat and mass transfer*, Vol. 40, No. 6, 1997, pp. 1481–1490.

[2]Moreno, O. A., Katyl, R. H., Jones, J. D., and Moschak, P. A., "Mass transfer of an impinging jet confined between parallel plates," *IBM J. RES. Develop.*, Vol. 37, No. 2, March 1993, pp. 143–155.

[3]Nishino, K., Samada, M., Kasuya, K., and Torii, K., "Turbulence statistics in the stagnation region of an axisymmetric impinging jet flow," *International journal of heat and fluid flow*, Vol. 17, 1996, pp. 193–201.

[4]Jamabunathan, K., Lai, E., Moss, M. A., and Button, B. L., "A review of heat transfer data for single circular jet impingement," *International Journal of heat and fluid flow*, Vol. 13, No. 2, June 1992, pp. 106–115.

[5]Sailor, D. J., Rohli, D. J., and Fu, Q., "Effect of variable duty cycle flow pulsations on the heat transfer enhancement for an impinging air jet," *International journal of heat and fluid flow*, Vol. 20, 1999, pp. 574–580.

[6]Mladin, E. C. and Zumbrunnen, D. A., "Local convective heat transfer to submerged pulsating jets," *International journal of heat and mass trasfer*, Vol. 40, No. 14, 1997, pp. 3305–3321.

[7]Zvirin, Y., "Heat transfer between a pulsating impinging jet and a flat surface," *Israel journal of technology*, Vol. 5, No. 1–2, 1967, pp. 152–169.

[8]Poh, H. J., Kumar, K., and Mujumdar, A. S., "Heat transfer from a pulsed laminar impinging jet," *International*

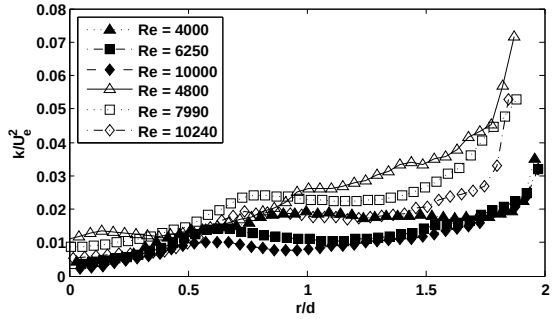

Figure 15. Effect of the Reynolds number on the mean turbulent kinetic energy near the impinging wall; closed symbols - steady jet, open symbols pulsed jet ($H/d = 3$, $St = 0.25$, $x/d = 2.85$)

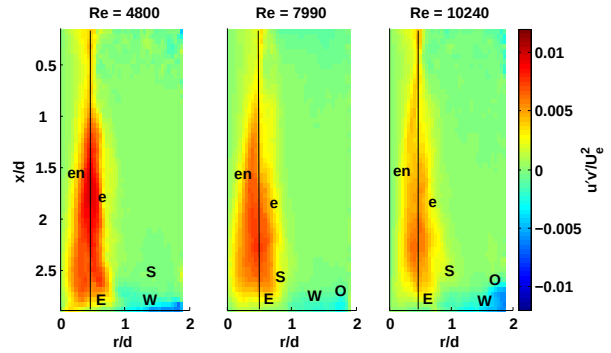

Figure 16. Effect of the Reynolds number on the Reynolds stress; entrainment (en), expulsion (e), ejection (E), sweep (S), wallward interaction (W), outward interaction (O) ($H/d = 3$, $St = 0.25$)

communications in heat and mass transfer, Vol. 32, 2005, pp. 1317–1324.

[9]Vejrazka, J., *Experimental study of a pulsating round impinging jet (Etude experimentale d'un jet circulaire impactant pulsant)*, Ph.D. thesis, Laboratoire des ecoulements geophysiques et industriels, Grenoble, December 2002.

[10]Hussain, A. K. M. F. and Zaman, K. B. M. Q., "Vortex pairing in circular jet under controlled excitation. Part 2. Coherent structure dynamics," *Journal of fluid mechanics*, Vol. 101, No. 3, 1980, pp. 493–544.

[11]Bremhorst, K. and Gehrke, P. J., "Measured Reynolds stress distributions and energy budgets of a fully pulsed round air jet," *Experiments in fluids*, Vol. 28, 2000, pp. 519–531.

[12]Aydore, S. and Disimile, P. J., "Natural coherent structure dynamics in near field of fully turbulent axisymmetric jet," *AIAA Journal*, Vol. 35, No. 7, July 1997.

[13]Gardon, R. and Akfirat, J. C., "The role of turbulence in determining the heat transfer characteristics of impinging jets," *International journal of heat and mass transfer*, Vol. 8, 1965, pp. 1261–1272.

[14]Ashforth-Frost, S., Jambunathan, K., Whitney, C. F., and Ball, S. J., "Heat transfer from a flat plate to a turbulent axisymmetric impinging jet," *Proc. instn. mech. engrs.*, Vol. 211, 1997, pp. 167–172.

[15]Baydar, E. and Ozmen, Y., "An experimental and numerical investigation on a confined impinging air jet at high Reynolds numbers," *Applied therman engineering*, Vol. 25, 2005, pp. 409–421.

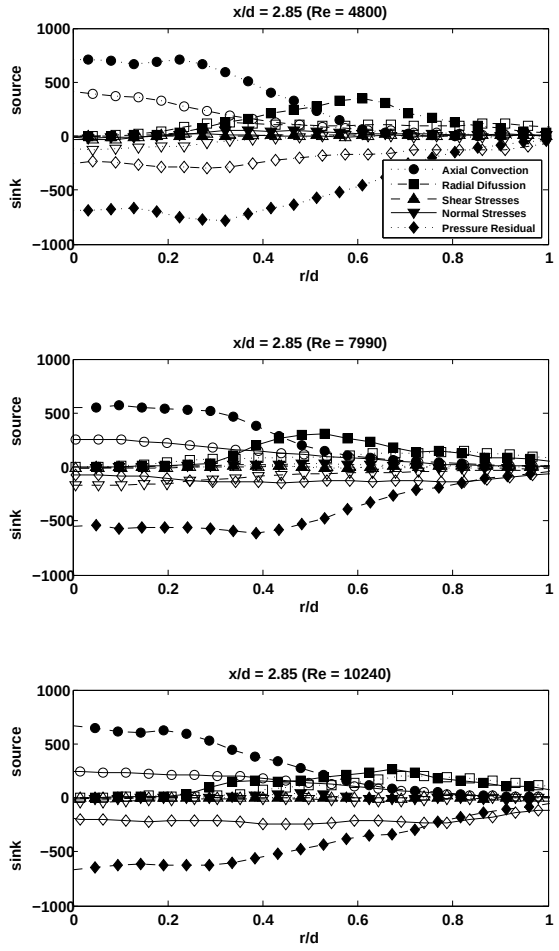

Figure 17. Effect of the Reynolds number on the mean axial momentum balance non-dimensionalised by d/U^2; closed symbols - steady jet, open symbols pulsed jet ($x/d = 2.85$, $St \approx 0.25$)